Title: Microglial MHC-I induction with aging and Alzheimer's is conserved in mouse models and humans

Authors: Collyn M. Kellogg[1,2,#], Kevin Pham[1,#], Adeline H. Machalinski[1], Hunter L. Porter[1], Harris E. Blankenship[3], Michael B. Stout[4], Heather C. Rice[2], Amanda L. Sharpe[5], Michael J. Beckstead[4,6], Ana J. Chucair-Elliott[1], Sarah R. Ocañas[1,2], Willard M. Freeman[1,2,6*]

Affiliations: [1]Genes & Human Disease Program, Oklahoma Medical Research Foundation, Oklahoma City, OK USA, [2]Department of Biochemistry & Molecular Biology, University of Oklahoma Health Sciences Center, Oklahoma City, OK USA, [3]Department of Physiology, University of Oklahoma Health Sciences Center, Oklahoma City, OK, USA, [4]Aging & Metabolism Program, Oklahoma Medical Research Foundation, Oklahoma City, OK USA, [5]Department of Pharmaceutical Sciences, University of Oklahoma Health Sciences Center, Oklahoma City, OK, USA. [6]Oklahoma City Veterans Affairs Medical Center, Oklahoma City, OK USA.

# - These authors contributed equally

To whom correspondence should be addressed: [*]Willard M. Freeman, Genes & Human Disease Program, Oklahoma Medical Research Foundation, 825 NE 13th Street, Oklahoma City, OK 73104, USA. E-mail address: bill-freeman@omrf.org

Acknowledgments: The content is solely the responsibility of the authors and does not necessarily represent the official views of the National Institutes of Health. This work was also supported by grants from the National Institutes of Health (NIH) P30AG050911, R01AG059430, DP5OD033443, T32AG052363, F31AG064861, F99AG079813, R21AG072811, and F31AG079620. This work was also supported in part by awards I01BX003906, IK6BX006033, and ISIBX004797 from the United States (U.S.) Department of Veterans Affairs, Biomedical Laboratory Research and Development Service. The Mount Sinai Brain Bank (MSBB) study data published here were data obtained from the AD Knowledge Portal (https://adknowledgeportal.org/). These data were generated from postmortem brain tissue collected through the Mount Sinai VA Medical Center Brain Bank and were provided by Dr. Eric Schadt from Mount Sinai School of Medicine. The authors would like to acknowledge Jay Hicks for assistance with figure preparation.

Abstract:

Major Histocompatibility Complex I (MHC-I) function in the CNS is still being determined after previously being thought to be absent from the brain. MHC-I expression increases with brain aging in mouse, rat, and human whole tissue analyses. Neuronal MHC-I expression has been proposed to regulate developmental synapse elimination and tau pathology in Alzheimer's disease (AD). However, the CNS cellular localization of MHC-I expression has been unclear. Across newly generated and publicly available ribosomal profiling, cell sorting, and single cell data, microglia were found to be the primary source of classical and non-classical MHC-I in mice and humans. TRAP-qPCR analysis of 3-6 m.o. and 18-22 m.o. mice revealed significant age-related induction of B2m, H2-D1, H2-K1, H2-M3, H2-Q6, and Tap1 in microglia but not in astrocytes and neurons. Across a timecourse from 12-23 m.o., microglial MHC-I gradually increases until 21 m.o. and then accelerates. MHC-I protein was also enriched in microglia and increased with aging. Expression of MHC-I binding Leukocyte Immunoglobulin-like (Lilr) and Paired immunoglobin-like type 2 (Pilr) receptors in microglia but not astrocytes or neurons opens the possibility of cell-autonomous signaling and are also increased with aging in mice and humans. Increased microglial MHC-I, Lilrs, and Pilrs were observed in mouse AD models and human data across numerous studies and in RNA-Seq of microglia from APP-PSEN1 mice. MHC-I expression occurred concurrently with p16 suggesting an association with cellular senescence. The conserved induction of MHC-I, Lilrs, and Pilrs with aging and AD open the possibility of cell-autonomous signaling to regulate microglial reactivation.

Introduction:

Historically, the brain has been proposed to be 'immune-privileged' due to the lack of/limited ability to develop adaptive immune responses to foreign antigens[1,2] and lack of conventional dendritic cells required to mount an adaptive immune response[3,4]. This difference between the brain and other peripheral organ systems led, in many cases, to a presumption that immune-related proteins expressed in other organ systems had no functional role in the CNS (except during viral infection and some pathological states where the BBB was highly compromised and the CNS recruits leukocytes to mount adaptive immune responses[5]). This has proven to be a mistaken assumption, as newer molecular biological and biochemical tools have identified multiple immune-related pathways expressed by CNS cells (i.e., class I major histocompatibility complex (MHC-I)[6], MHC-II[7], complement components [8,9], and toll-like receptors (TLRs)[10]). The characterization of these molecules like as 'immunological' comes from their initial discovery in the immune system. Evolving evidence suggests that many of these 'immune' genes are functionally pleiotropic, with different functions in different cellular milieus[11]. For example, mice deficient in complement components display defects in CNS synapse elimination[12,13] but this process is independent of the classical role of complement in innate immune clearance of microbes or adaptive immune detection of non-self antigens. Similarly, deficiency of the MHC-I molecule β2-microglobulin (B2m) leads to higher cortical synapse density in the mouse brain[14]. We would propose that these 'immunological' molecules in the CNS are better classified as signaling molecules that work in both *cis* (cell-autonomous signaling within one cell) and *trans* (signaling between two cells, such as across synapses) to regulate brain function, in addition to some more conventional immunological roles. This fits with a more complete and nuanced contemporary view of immune privilege[15,16].

The MHC pathways are elements of the adaptive and innate, immune systems, with Class I canonically presenting intracellular antigens for viral surveillance and Class II presenting extracellular antigens for bacterial surveillance. While traditionally/canonically thought to be unexpressed in the brain[17,18] evidence of MHC-I expression by brain resident cells, principally glia, has been shown for decades[19,20]. MHC-I is further divided into classical I/Ia and non-classical groupings Ib in which the non-classical genes exhibit a more restricted expression to specific cell types and are less polymorphic[21]. There are not exact homologs between each murine and human MHC-I gene but Class I in humans encompasses HLA-A,-B,-C, and in Mice H2-D,-K, and forms, while Class Ib in human are HLA-E,-F,-G, and mice are H2-M,-T,-Q[22,23]. Peptides for presentation by

MHCs are generated initially in the cytosol by the proteasome[24]. These peptides are transported into the endoplasmic reticulum (ER) by the transporter associated with antigen processing (Tap1 and Tap2). Peptides are then loaded onto MHCs by tapasin (Tapbp, transporter associated with antigen processing binding protein). MHC-I can also cross-present exogenous antigens[25]. For MHCs to localize to the cell surface, they must be associated with B2m[26]. MHC-I is canonically recognized by the T-Cell receptor (TCR) to mount adaptive immune responses in an antigen-dependent manner[27]. However, a wide variety of paired immune receptors can also bind MHC-I in what is likely antigen-dependent and antigen-independent manners (though many questions remain to be answered in this signaling process)[28-30]. These paired receptor families include leukocyte immunoglobulin-like receptors (Lilr)[31,32], paired immunoglobin-like type 2 receptors (Pilr)[33], and C-type lectin-like receptors (Clec)[34] most of which contain ITAMs (Immunoreceptor Tyrosine-based Activation Motifs) and ITIMs (Immunoreceptor Tyrosine-based Inhibition Motifs) that can induce activational or inhibitory signals in the recognizing cell[35].

MHC-I expression, after first being described as absent from the CNS[17], especially neurons[18], was ascribed to neurons in developmental studies[20,36] and then in the adult but without expression in microglia or astrocytes[37,38] except in pathological states. Much of the interest in MHC-I and potential non-TCR mediated signaling came from developmental [39-42] literature and proposed a neuronal source and function on MHC-I. Recently, a neuron-centric MHC-I function in AD was reported[43] where MHC-I, driven by ApoE expression, drives neurodegeneration. Subsequent studies have ascribed MHC-I expression to astrocytes[44], microglia[45], and other CNS cell types[46]. However, scRNA-Seq studies of microglial molecular phenotypes include MHC-I components and paired receptor family members[47-49] as key markers of Disease Associated Microglia (DAMs) and other subtypes (recognizing that the microglial state terminology has become overlapping and occasionally misleading[50]).

Previously, we have reported MHC-I induction with aging in mice and rats[51,52] and this study seeks to clarify the cells expressing MHC-I in the brain and the localization of changes in MHC-I with aging and AD, in mice and humans. Data across multiple cohorts of animals/subjects and from a variety of methods was combined to increase the rigor of analyses and avoid technical confounds. Microglia were identified as the primary sources of MHC-I with aging and AD and the co-expression of MHC-I with paired immunoglobulin like

receptors that can bind MHC-I opens the possibility of cell-autonomous regulation of microglial phenotype by MHC-I with aging and disease.

Methods:

Mice: All animal procedures were approved by the Oklahoma Medical Research Foundation (OMRF). Mice were purchased from the Jackson Laboratory (Bar Harbor, ME), bred, and housed at the OMRF, under SPF conditions in a HEPA barrier environment. In separate breeding strategies, as described previously[53], Aldh1l1-Cre/ERT2$^{+/wt}$ males (stock number # 031008)[54], Cx3cr1^{Jung}-Cre/ERT2$^{+/+}$ (stock # 20940)[55], Cx3cr1^{Litt}-Cre/ERT2$^{+/+}$ (stock #021160)[56], and CamkII□-Cre/ERT2$^{+/wt}$ (stock # 012362)[57] were mated with NuTRAP$^{flox/flox}$ females (stock # 029899)[58] to generate the desired progeny, Aldh1l1-cre/ERT2$^{+/wt}$; NuTRAP$^{flox/wt}$ (Aldh1l1-NuTRAP^{+}), Cx3cr1^{Jung}-cre/ERT2$^{+/wt}$; NuTRAP$^{flox/wt}$ (Cx3cr1^{Jung}-NuTRAP^{+}), Cx3cr1^{Litt}-cre/ERT2$^{+/wt}$; NuTRAP$^{flox/wt}$ (Cx3cr1^{Litt}-NuTRAP^{+}), and CamkIIα-cre/ERT2$^{+/wt}$; NuTRAP$^{flox/wt}$ (CamkIIa-NuTRAP^{+}). Founders for both APP-PSEN1 (MMRC #034832)[59] and control mice were obtained from Dr. Salvatore Oddo, who had backcrossed them for more than 12 generations and maintained them on a 129/SvJ background as previously described [60]. Local breeding of APP-PSEN1 and control mice was done in parallel. DNA was extracted from mouse ear punch samples for genotyping. At 3 months of age, unless otherwise noted, mice received a daily intraperitoneal (ip) injection of tamoxifen (Tam) solubilized in 100% sunflower seed oil by sonication (100□mg/kg body weight, 20□mg/ml stock solution, #T5648; Millipore Sigma, St. Louis, MO) for five consecutive days[53]. TAM dependent cre induction at 3 months of age does not lead to long lasting changes in brain gene expression[61] and avoids potential confounds of early post-natal TAM administration[62]. Based on an average weight of 20 g per mouse, each daily injection of Tam consisted of 100□µl of 20□mg/ml stock solution. Adjustments were made for mice that significantly deviated from the average weight. Mice were euthanized by cervical dislocation, followed by rapid decapitation, in line with the AVMA Guidelines for the Euthanasia of Animals.

Mouse Genotyping: DNA was extracted from ear tissue by incubating samples in 50 nM NaOH at 95°C for 1 hour, after which reaction was neutralized by adding 30 uL 1 M Tris HCl (pH: 7.4). Processed samples were then genotyped using a touchdown PCR reaction (94°C hotstart for 2 min, 10 cycles of touchdown (94°C 20 sec, 65°C 15 sec (-0.5C per cycle decrease per cycle), 68°C,10 sec) followed by 28 cycles of amplification (94°C 15 sec, 60°C 15 sec, 72°C 10 sec) with the listed primer sets (Supplementary Table 1).

Mice were collected at the ages described in each experiment. Euthanasia prior to tissue harvesting was carried out either by cervical dislocation, or by cardiac perfusion with phosphate buffered saline (PBS), upon deeply anesthetizing mice with ketamine/xylazine. The primers used for genotyping (Integrated DNA Technologies, Coralville, IA) are included in Supplemental Table 1.

TRAP isolation: TRAP isolation from hippocampus was performed as previously described[53]. Minced tissue was Dounce homogenized (#D8938; MilliporeSigma) in 1.5 ml chilled homogenization buffer (50 mm Tris, pH 7.4; 12 mm $MgCl_2$; 100 mm KCl; 1% NP-40; 1 mg/ml sodium heparin; 1 mm DTT; 100 µg/ml cycloheximide (#C4859-1ML, MilliporeSigma); 200 units/ml RNaseOUT Recombinant Ribonuclease Inhibitor (#10777019; Thermo Fisher Scientific); 0.5 mm Spermidine (#S2626, MilliporeSigma), 1× complete EDTA-free Protease Inhibitor Cocktail (#11836170001; MilliporeSigma)). Homogenates were transferred to 2 ml round-bottom tubes and centrifuged at 12,000 × *g* for 10 min at 4°C. 100 µl of supernatant was saved as TRAP "Input." Remaining supernatant was transferred to a 2-ml round-bottom tube and incubated with 5 µg/µl of anti-GFP antibody (ab290; Abcam) at 4°C with end-over-end rotation for 1 h. Dynabeads Protein G for IP (#10003D; Thermo Fisher Scientific) were pre-washed three times in 1-ml ice-cold low-salt wash buffer (50 mm Tris, pH 7.5; 12 mm $MgCl_2$; 100 mm KCl; 1% NP-40; 100 µg/ml cycloheximide; 1 mm DTT). The homogenate/antibody mixture was transferred to the 2-ml round-bottom tube containing the washed Protein-G Dynabeads and incubated at 4°C with end-over-end rotation overnight. Magnetic beads were collected (DynaMag-2 magnet) and the unbound-ribosomes and associated RNA discarded. Beads and GFP-bound polysomes were then washed 3X with 0.5 ml of high-salt wash buffer (50 mm Tris, pH 7.5; 12 mm $MgCl_2$; 300 mm KCl; 1% NP-40; 100 µg/ml cycloheximide; 2 mm DTT). Following the last wash, 350 µl of buffer RLT (QIAGEN) supplemented with 3.5 µl 2-β mercaptoethanol (#444203, MilliporeSigma) was added directly to the beads and incubated with mixing on a ThermoMixer (Eppendorf) for 10 min at room temperature. The beads were magnetically separated and the supernatant containing the target bead-bound polysomes and associated RNA was transferred to a new tube. A total of 350 µl of 100% ethanol was added to the tube ("TRAP" fraction: enriched in transcriptome associated to eGFP-tagged ribosomes) and loaded onto a RNeasy MinElute column (QIAGEN). RNA was isolated using RNeasy Mini kit (#74104, QIAGEN), according to manufacturer's instructions. RNA was quantified with a Nanodrop One^c spectrophotometer (#ND-ONEC-W, Thermo Fisher

Scientific) and its quality assessed by HSRNA ScreenTape (#5067-5579, Agilent Technologies) with a 4150 Tapestation analyzer (#G2992AA, Agilent Technologies).

RT-qPCR: Relative gene expression levels were quantified by qPCR as previously described [63,64]. cDNA was synthesized with the ABI High-Capacity cDNA Reverse Transcription Kit (Applied Biosystems Inc., Foster City, CA) from 25 ng of purified RNA. qPCR was performed with gene-specific primer probe fluorogenic exonuclease assays (TaqMan, Life Technologies, Waltham, MA, Supplemental Table 2) and the QuantStudio 5 Real-Time PCR System (Applied Biosystems). Relative gene expression (RQ) was calculated with Expression Suite v 1.3 software using the $2^{-\Delta\Delta}$Ct analysis method with GAPDH as an endogenous control. Statistical analysis of the qPCR data was performed using GraphPad Prism 9 (San Diego, CA). One or Two-way ANOVA analyses were performed as appropriate followed by the Tukey's multiple comparison test ($p < 0.05$) with a Benjamini Hochberg Multiple Testing correction applied within each tissue.

Single cell suspension: Hippocampi were rinsed in ice-cold D-PBS containing calcium, magnesium, glucose, and pyruvate (#14287-072, Thermo Fisher Scientific), sliced into four sagittal sections on a chilled, metal block and placed into ice-cold gentleMACS C-tubes (#130-093-237, Miltenyi Biotec), containing 1950 µl of papain-based, Enzyme Mix 1. For each reaction, Enzyme Mix 1 was created by combining 50 µl of Enzyme P with 1900 µl of buffer Z, while Enzyme Mix 2 was created by combining 10 µl of Enzyme A with 20 µl of buffer Y per reaction, with all reagents included in the Adult Brain Dissociation kit (#130-107-677, Miltenyi Biotec). Transcription and translation inhibitors were included during cell preparation to prevent *ex vivo* activational artifacts, as previously described[65]. Actinomycin D (#A1410, MilliporeSigma) was reconstituted in DMSO to a concentration of 5 mg/ml before being aliquoted and stored at −20°C protected from light. Triptolide (#T3652, MilliporeSigma) was reconstituted in DMSO to a concentration of 10 mm before being aliquoted and stored at −20°C protected from light. Anisomycin (#A9789, MilliporeSigma) was reconstituted in DMSO to a concentration of 10 mg/ml before being aliquoted and stored at 4°C protected from light. 2 µl each of actinomycin D, triptolide, and anisomycin stocks were added to the initial Enzyme Mix 1 before dissociation for a final concentration of 5 µg/ml, 10 µm, and 10 µg/ml, respectively. Each sample then had 30 µl of Enzyme Mix 2 added before being mechanically dissociated for 30 min at 37°C on the gentleMACS Octo Dissociator with Heaters (#130-096-427, Miltenyi Biotec) using the 37C_ABDK_02 program. Following enzymatic and mechanical dissociation, the C-tubes were quickly spun in a chilled (4°C) Allegra-30R centrifuge (#B08708,

Beckman Coulter) with an SX4400 swinging bucket rotor to collect the samples in the bottom of the tubes. Next, samples were resuspended and passed through a pre-wet 70 µm MACS SmartStrainer (#130-110-916, Miltenyi Biotec) and collected in a 50-ml conical tube (#21008-178, VWR International). The C-tubes were washed with 10 ml of ice-cold D-PBS and the washed volume was passed through the 70 µm MACS SmartStrainer. The cells were then pelleted by centrifugation at 300 × *g* for 10 min at 4°C. Following centrifugation, the supernatant was aspirated and debris was removed using the Debris Removal solution (#130-109-398, Miltenyi Biotec) provided in the Adult Brain Dissociation kit (#130-107-677, Miltenyi Biotec). Briefly, cells were resuspended in 1.55 ml of ice-cold D-PBS and passed to a 5-ml round bottom tube (#22171606, FisherScientific) and 450 µl of cold Debris Removal solution was mixed into the cell suspensions. Next, 2 ml of D-PBS was gently overlaid on top of the cell suspension, ensuring the layers did not mix. Centrifugation at 3000 × *g* for 10 min at 4°C separated the suspension into three phases, of which the top two phases were aspirated. The cell pellet was gently resuspended in 5 ml of ice-cold D-PBS before centrifugation at 1000 × *g* for 10 min at 4°C. After aspirating the supernatant completely, the cells were resuspended in 1 ml 0.5% BSA (#130-091-376, Miltenyi Biotec) in D-PBS and filtered through a 35-µm filter (#352235, Fisher Scientific). A 100 µl aliquot of cells was retained as “Cell-Input” for flow cytometric and RNA sequencing (RNA-Seq) analyses[65].

AutoMACS: Hippocampal single cell suspensions were pelleted at 300 × g for 10 min at 4°C and resuspended in 90 µl of 0.5% BSA in D-PBS with 10 µl of CD11b (Microglia) MicroBeads (#130-093-636, Miltenyi Biotec) per 10^7 total cells. After gentle pipette mixing, cells were incubated for 15 min at 4°C in the dark. Cells were washed with 1 ml of 0.5% BSA in D-PBS and pelleted at 300 × g for 10 min at 4°C. The cell pellet was resuspended in 500 µl of 0.5% BSA in D-PBS. After priming the autoMACS Pro Separator (#130-092-545, Miltenyi Biotec), sample and collection tubes were placed in a cold MACS Chill 5 Rack (#130-092-951, Miltenyi Biotec) with both positive and negative fractions being collected. The double-positive selection (Posseld) program (i.e., positive fraction cells are then run over a second magnetic column for higher purity) was used to elute highly pure CD11b+ cells in 500 µl of autoMACS Running buffer (#130-091-221, Miltenyi Biotec). Following separation, the positive and negative fractions were reserved for further applications and analysis.

RNA-Seq: Directional RNA-Seq libraries (NEBNext Ultra II Directional RNA Library, New England Biolabs, Ipswich, MA NEB#E7760) were made according to the manufacture's protocol for 2 to 100 ng RNA. $CD11b^+$ cells from magnetic bead isolation were used to create individual RNA-Seq libraries (no pooling of samples was performed). Poly-adenylated RNA was captured using NEBNext Poly(A) mRNA Magnetic Isolation Module (#NEBE7490). Following mRNA capture, mRNA was eluted from the oligo-dT beads and fragmented by incubating with the First Strand Synthesis Reaction buffer and Random Primer Mix (2×) from the NEBNext Ultra II Directional Library Prep Kit for Illumina (#NEBE7760; New England Biolabs) for 15 min at 94°C. First and second strand cDNA synthesis were performed sequentially, as instructed by the manufacturer's guidelines. After purification of double-stranded cDNA with 1.8× SPRISelect Beads (#B23318, Beckman Coulter), purified cDNA was eluted in 50 µl 0.1× TE buffer and subjected to end prep. The NEBNext Adaptor was diluted 1:100 in Adaptor Dilution buffer (provided) before ligating the adaptor to the cDNA. After purifying the ligation reaction with 0.9× SPRISelect Beads (#B23318, Beckman Coulter), cDNA was eluted in 15 µl of 0.1× TE (provided). Next, cDNA libraries were amplified with 16 cycles of PCR using the NEBNext Ultra II Q5 Master Mix (provided) and unique index primer mixes from NEBNext Multiplex Oligos for Illumina Library (#E6609L, New England Biolabs). Libraries were purified with 0.9× SPRISelect Beads (#B23318, Beckman Coulter) and then sized with HSD1000 ScreenTapes (#5067-5584; Agilent Technologies). Libraries had an average peak size of 316 bp. Libraries were quantified by Qubit 1× dsDNA HS Assay kit (#Q33230, Thermo Fisher Scientific). The libraries for each sample were pooled at 4 nm concentration and sequenced using an Illumina NovaSeq 6000 system (S4 PE150). The entirety of the sequencing data are available for download in FASTQ format from NCBI Gene Expression Omnibus (to be included on acceptance).

Flow cytometry: For flow cytometric analysis, cell preparations were taken for analysis on the MACSQuant Analyzer 10 Flow Cytometer. Cell were stained with CD11b-APC (M1/70, #130-113-793, Miltenyi Biotec) and CD45-VioBlue (REA737, #130-110-802, Miltenyi Biotec) either H-2-PE (REA857, #130-112-481) or H-2-FITC (M1/42, #125508). Following staining, cells were resuspended in 250 µl of 0.5% BSA/D-PBS and run on the MACSQuant Analyzer 10 Flow Cytometer. Data was analyzed using MACSQuantify v2.13.0 software.

Immunohistochemistry: Brain samples were fixed for 4 h in 4% PFA, cryoprotected by sequential incubations in PBS containing 15% and 30% sucrose, and then frozen in Optimal Cutting Temperature medium (#4583, Tissue-Tek). Twelve µm-thick sagittal sections were cryotome-cut (Cryostar NX70, Thermo Fisher Scientific).

Tissue sections were rinsed with PBS containing 1% Triton X-100, blocked for 1 h in PBS containing 10% normal donkey serum, and processed for fluorescence immunostaining and downstream analysis. The primary antibodies included rabbit anti-GFP (#ab290, 1:100, Abcam), rat anti-CD11b (#C227, Clone M1/70, 1:100, Leinco Technologies), and rat anti-B2m (#555299, Clone S19.8, 1:100, BD Biosciences). Sequential imaging was performed on an Olympus FluoView confocal laser-scanning microscope (FV1200; Olympus) at the Dean McGee Eye Institute imaging core facility at OUHSC. Microscope and FLUOVIEW FV1000 version 1.2.6.0 software (Olympus) settings were identical for samples using the same staining-antibody combination and at same magnification. The experimental format files were oib. The Z-stack generated was achieved at 1.26-µm step size with a total of eight optical slices at 20× magnification (2× zoom).

Data Analysis: Following sequencing, reads were trimmed and aligned before differential expression statistics and correlation analyses in Strand NGS software package (v4.0; Strand Life Sciences). Reads were aligned against the full mm10 genome build (2014.11.26). Alignment and filtering criteria included the following: adapter trimming, fixed 2-bp trim from 5′ and 2□bp from 3′ ends, a maximum number of one novel splice allowed per read, a minimum of 90% identity with the reference sequence, a maximum 5% gap, and trimming of 3′ end with Q□<□30. Alignment was performed directionally with Read 1 aligned in reverse and Read 2 in forward orientation. All duplicate reads were then removed. Normalization was performed with the DESeq2 algorithm. Transcripts with an average read count value >5 in at least 100% of the samples in at least one group were considered expressed at a level sufficient for quantitation per tissue and those transcripts below this level were considered not detected/not expressed and excluded, as these low levels of reads are close to background and are highly variable. For statistical analysis of differential expression, a t-test between control and APP-PSEN1 with Benjamini–Hochberg multiple testing correction (BHMTC). For those transcripts meeting this statistical criterion, a fold change >|1.25| cutoff was used to eliminate those genes which were statistically significant but unlikely to be biologically significant and orthogonally confirmable because of their very small magnitude of change. Visualizations of hierarchical clustering and principal component analyses (PCAs) were performed in Strand NGS (version 4.0). Upset plots were created using ComplexHeatmap v2.14.0 package in RStudio 2022.07.2 Build 576 with R v4.2.1. Gene expression data and associated annotations of age and tissue were downloaded in bulk from the Tabula Muris[66] or Atlas of the Aging Mouse Brain[67]. Only counts greater than 1 were considered for the plot. For human GeTX data across tissues and ages, count-level expression

data were quantile normalized and log-transformed before analysis. Significance of age-association was determined using Pearson correlation computed using Scipy stats' pearsonr function[68]. Relationships were visualized using seaborn (Waskom, M. et al., 2017. *mwaskom/seaborn: v0.8.1 (September 2017)*, Zenodo. Available at: https://doi.org/10.5281/zenodo.883859.)

Results

RNA-Seq data from bulk FACS or immunopanned young (~2 m.o.) sorted astrocytes (Aldh1l1+), neurons (L1cam+), and microglia (CD45+) from the BrainRNASeq[69] database were examined for Class 1, Class 1b, and antigen processing components of the MHC-I pathway. Limited to no expression was observed in astrocytes or neurons, with highest levels of expression in microglia (**Figure 1**). To examine cell-type specific expression by an independent technical method, Translating Ribosome Affinity Purification (TRAP)[70] isolated RNA from astrocytes (Aldh1l1-NuTRAP), neurons (CamkIIα-NuTRAP), and microglia (Cx3cr1-NuTRAP) from hippocampus of young (~3 m.o.) mice from our previous studies[53] was compared. Again, highest expression was observed in microglia. A difference between sorted cells and ribosomal profiling data is that transcripts translated in distal cellular processes are retained while these are generally lost in cell sorting data. Data comparing somally enriched and distal process enriched microglial transcripts[71] identified B2m, H2-D1, H2-K1, and H2-M3 as all significantly enriched in distal processes of microglia.

To examine hippocampal expression of MHC-I pathway components with aging in a cell-type specific manner, RNA was TRAP isolated from our NuTRAP models for astrocytes (Aldh1l1-cre), neurons (CamkIIα-cre), and microglia (Cx3cr1-cre) young (3-6 m.o.) and old (18-22 m.o.), male and female mice and analyzed by RT-qPCR. Genes were selected based on existing tissue level RNA-Seq and scRNA-Seq analyses of mouse brain aging. Robust increases in B2m as well as Class I (H2-D1, H2-K1) and non-classical Class Ib (H2-M3, H2-Q6) MHCs and Tap complex member Tap1 MHC-Is expression were observed in microglia, in both males and females with age (**Figure 2A**). A few, small magnitude age and sex differences were observed in astrocytes and neurons.

With the concentration of age-related changes to microglia, a timecourse of MHC-I pathway induction was examined across 12 – 23 m.o. female Cx3cr1^{Litt}-NuTRAP mice by TRAP-qPCR. A steady increase in MHC-I pathway expression was observed across all genes (**Figure 3**). These data demonstrate a reproducible increase in microglial MHC-I with aging that accelerates as mice near two years of age.

To extend these gene expression findings, cell surface MHC-I expression was examined. Antibodies that recognize specific MHC-I β chains are limited but pan-H2 antibodies have been widely used[72]. To validate which brain cells express cell surface MHC-I, hippocampal cells from wild type mice (~5-7 m.o.) were gated on CD11b^{+} and CD45^{mid} for microglial cells and staining for pan-H2 was assessed (**Figure 4A**). Across all cells

less than 10% were pan-H2 positive while ~95% of microglia were pan-H2 positive. Only ~5% of negative gate cells were pan-H2 positive which likely includes some microglia as the gating strategy for microglia is not 100% efficient. To examine whether cell surface MHC-I is altered with aging, hippocampal cells from wild-type 5 m.o. and 24 m.o. male and female mice were gated on $CD11b^{+}$ and $CD45^{mid}$ and again showed enrichment for MHC-I and increased fluorescent intensity in Old as compared to Young, a finding which was observed with two different antibodies (**Figure 4B&C**). Similarly, NuTRAP mice were gated on the GFP^{+} signal and demonstrated increased cell surface expression of MHC-I in 24 m.o. mice as compared to 7-9 m.o. mice (**Figure 4D**). B2m induction with aging was confirmed in hippocampal tissue sections from $Cx3cr1^{Jung}$-NuTRAP mice (**Figure 5**).

To assess MHC-I cellular expression and regulation with aging, first the Genotype-Tissue Expression Project (GTeX)[73] was collected with age and tissue annotations. MHC-I components were assessed as a function of age in blood, brain, liver, lung, and muscle samples. A consistent induction with aging was observed in brain, lung, and muscle but not in blood or liver annotated samples (**Figure 6A**). RNA-Seq data from human brain sorted cells[74] was assessed for MHC-I expression and while B2m was expressed across cell types, other MHC-I components were almost exclusively expressed in microglia (**Figure 6B**). Microglia from Adult (average age 53 y.o.) and Aged (average age 93 y.o.) fresh brain samples were isolated by magnetic bead enrichment for CD11b+ cells followed by FACS for $CD11b^{+}$/$CD45^{+}$ and RNA-Seq performed[75]. MHC-I components, B2m and canonical and non-canonical MHC-I) were induced with aging (**Figure 6C**).

To extend these findings and examine MHC-I expression in individual cells the Tabula Muris[66] and the Atlas of the Aging Mouse Brain[67] were retrieved and examined for co-expression of MHC-I components. Almost all individual microglial expressed both the invariant β chain (B2m) and at least one α chain needed to make a functional, cell surface MHC-I (**Figure 7A**). Very limited numbers of astrocytes or neurons were found to express both α and β chains (**Figure 7B&C**). During these analyses it was observed that many microglial also expressed paired immunoglobulin-like receptors (Lilra5, Lilrb4, Pilra, Lilrb3 (aka, PirB)). This was of note as these are potential receptors for MHC-I[42]. No expression of the receptors was observed in astrocytes or neurons. This opens the potential for MHC-I singling in microglia in a cell autonomous manner and in a microglia-to-microglia cell non-autonomous manner. Therefore the expression of paired immunoglobulin-like receptors across cell types and with aging was examined.

In the same cell sorting and translatome datasets as before (**Figure 1**), Pilr and Lilr expression was restricted to microglia (**Figure 8A**). Across microglial, astrocyte, and neuronal TRAP-qPCR aging data, receptor expression of Lilrb3, Lilrb4, and Pilra were elevated with aging in microglia but not astrocytes or neurons. In fact, most receptors were not detected in TRAP isolated fractions from these mice. Extending to a time course of microglial aging, Lilrb3 and Lilrb4 increased at 18-21 m.o. as measured by TRAP-qPCR (**Figure 8E**).

In human GTeX data, Lilr and Pilr expression increased as a function of age in brain with a variety of patterns observed in other tissues (**Figure 9A**). Cell sorting data from humans also shows restricted expression of these receptors to microglia (**Figure 9B**). In human microglia Lilr and Pilr expression increased with age (**Figure 9C**). Thus microglial enriched expression of Pilrs and Lilrs is conserved in mice and humans and increases with age.

AD is one of the most common and debilitating age-related neurodegenerations. To extend these findings of age-related microglial MHC-I and paired immunoglobulin-like receptor induction, a variety of mouse models rTg4510[48], AppNL-G-F[48,77], App-SAA, and 5xFAD[79,80] with microglial specific expression data were examined for altered expression of MHC-I and paired immunoglobulin-like receptors. A consistent microglial up-regulating of almost all the genes examined was evident, across models and technical methods (magnetic bead isolation and FACS and bulk, scRNA and snRNA-Seq) (**Table 1**).

To further extend these findings we isolated microglial from 12 m.o. APP-PSEN1 hippocampus by $CD11b^{+}$ microbeads and performed RNA-Seq. The transcriptomic patterns of APP-PSEN1 microglia differed from controls (**Figure 10A**) and 4,389 genes demonstrated differential expression (**Figure 10B**). Using z-scores (**Figure 10C**) and GSEA analysis (**Figure 10D**) of microglial phenotype markers, a shift in favor of proliferative region associated microglia (PAMs), disease associated microglia (DAMs), and white matter associated microglial (WAMs) were evident in both analyses. As well, homeostatic markers were depleted and notably lipid droplet associated microglia (LDAM) markers were suppressed. For the MHC-I genes of interest, an upregulation of B2m, H2-D1, H2-K1, and H2-M3 was observed as was an induction of Lilrb4 and intriguingly a suppression of Pilra (**Figure 10E**). In parallel we examined human AD microglial data [76,80,81] from tissue, sorted cells or snRNA-Seq data and again found induction of MHC-I and paired immunoglobulin-like receptors in cases as compared to controls (**Table 2**).

An observation from the APP-PSEN1 RNA-Seq data was an increase in the expression level of the senescence marker p16INK4A in microglia (**Figure 11D**). TRAP-qPCR was performed on the aging samples described above and a significant induction of p16 with aging was observed in microglia but no expression was detected in astrocytes or neurons (**Figure 11A**). In timecourse samples, p16INK4A expression followed a similar pattern as the MHC-I genes with a gradual increase that accelerated at 23 m.o. The similar patterns of expression across the time course study was further examined in a correlation analysis with high degrees of correlation across genes examined (**Figure 11C**).

The common regulation of these genes in microglia across aging and AD and in mouse and man provides a compelling result and to determine if these genes may warrant further mechanistic study, TREAT-AD scores[82] were collected for each of these genes and compared to the distribution of all annotated genes (**Figure 12**). The TREAT-AD score was developed as part of NIH consortia to prioritize AD targets for investigation and potentially therapeutic targets. The TREAT-AD score is a combination of genetic association, predicted variant

impact, and associated dementia phenotypes, paired with extensive sets of transcriptomic and proteomic of AD-related expression changes.

However interpretation of these results is hindered by lack of basic biological knowledge on microglial MHC-I and its signaling partners suggesting that mechanistic studies of microglial function are needed in the field. The potential impact of studies in this pathway is supported by high TREAT-AD scores (**Fig. 2**) for many of the genes in this pathway[82]

Discussion:

These results demonstrate that the principle source of MHC-I in the CNS is microglia and that with aging and in human AD samples or in mouse models of AD microglial MHC-I increases in expression at the transcript, translating transcript, and protein level. This provides a cellular context to previous tissue level analyses with aging[51,52]. The consistency of these finds across studies, technical methods, and microglial isolation approaches engenders confidence in the results.

The functional consequences, if any, of microglial MHC-I induction with aging and AD remain to be determined. The canonical signaling partner for MHC-I is the T-cell Receptor (TCR). The potential for T-cell infiltration into the brain with aging and AD has been a question in the field for at least a decade[83,84]. Aging

causes an increase in CD8+ T-cells in mice[85] which has subsequently been characterized as tissue resident T-cells (Trm) but the characterization of infiltrating T-cells with aging and AD is an ongoing and controversial topic (for review see[84,86-88]). The data on T-cell infiltration into the parenchyma with non-pathological aging is varied with reports ranging from no or limited infiltration to significant numbers [89-91]. While this question remains to be definitively answered, microglial reactivation could serve to recruit T-cells[92] and microglial proximity to pericytes and endothelial cells suggest they could present MHC-I to infiltrating T-cells[93]. In turn, T-cells could modulate microglial phenotype[94]. In the APP/PSEN1 model used here, infiltration of T-cells has been reported[95] which means one possibility is that the induction of MHC-I observed here could be to signal to T-cells. Antigens can exit the brain through the dural sinus[96] for positive selection but if this occurs with aging or AD[97] is still being determined. Nonetheless, the possibility exists for antigen-specific signaling of MHC-I to T-Cells with aging and AD though much further investigation is needed.

A principle finding from this study is that antigen-independent MHC-I receptors: leukocyte immunoglobulin-like receptor subfamily receptors (Lilr)[31,32], and paired immunoglobulin-like type 2 receptors (Pilrs)[33], are present and induced in microglia with aging and AD. These receptors are almost exclusively restricted to microglia in the CNS. These receptors contain ITAMs (Immunoreceptor Tyrosine-based Activation Motifs) and ITIMs (Immunoreceptor Tyrosine-based Inhibition Motifs) that can induce activational or inhibitory signals in the recognizing cell[35]. ITAMs are familiar to AD research through Trem2 effector Tyrobp/DAP12 which contains an ITAM motif[98]. ITAMs activate and ITIMs inhibit Syk activity, a central controller of microglial phenotype[99-101]. Lilr and Pilr receptors can bind MHC-I[32,102] in antigen-dependent and antigen-independent manners though many questions remain to be answered in this signaling process[28-30]. Thus microglial MHC-I could be signaling in a cell-autonomous manner (or in microglia-microglial contacts) to regulate microglial phenotype through these receptors, ITIMs/ITAMs and Syk. This concept is support by data such as the ITIM containing CD22 regulating microglial phagocytosis[103]. This area of investigation clearly warrants further investigation.

Our microglial hypothesis differs but is not in opposition to the neuron-centric MHC-I function in AD recently reported[43] that MHC-I, driven by ApoE expression, drives neurodegeneration. As they show, ApoE expression is highest in microglia and astrocytes with a small minority of neurons expressing low levels of ApoE. Global knock-in of human ApoE4 and then knockout of ApoE specifically in neurons reduced expression

of some MHC-I genes (H2-Ts, H2-D1, but not H2-K1). We propose that their studies showing protection from p-tau in a non cell-specific B2m knockout model are actually mediated through microglia instead of neurons as the vast majority of B2m is in microglia. Taking our cell type specific TRAP-Seq data across ages and sexes, we find that ApoE levels are highly correlated to MHC-I components B2m, H2-D1, and H2-K1 in microglia and neurons but the expression level is an order of magnitude higher in microglia than neurons (data not shown). Thus we would propose a microglial focus to MHC-I actions in brain aging and AD where we have found robust and consistent upregulation of MHC-I and potential receptors.

Lastly the finding of the canonical senescence marker, p16INK4A, as also induced in microglia, but not other cell types examined, could point to another function of microglial MHC-I. In the periphery, MHC-I expression in senescent fibroblasts has been demonstrated to be a mechanism by which these cells avoid immune clearance through the ITIM containing receptor NKG2A on NK and T cells[104]. Microglial senescence has been described[105] and is attributed to replicative exhaustion [106]. In fact, an analysis of p16INK4A^{+} versus negative microglia show induction of the MHC-I, Lilr, and Pilr genes observed here. The nature of microglial 'senescence'[107] still requires more study and it remains to be determined if MHC-I induction is a result or cause of microglial senescence, or if senescence is even the best categorization of this phenotypic state of microglia.

In conclusion these data show that microglial express MHC-I at much higher levels than other CNS cell types examined in mice and man. Furthermore, MHC-I is induced in microglia with aging and AD (or AD models) in mice and humans. While the signaling partner(s) of MHC-I are unknown, we report that microglia co-express Lilr and Pilr receptors that could bind MHC-I to transduce inhibitory or excitatory signals to microglia. Intriguingly, these receptors are also induced in microglia with aging and AD, identifying a potential new pathway of microglial phenotype regulation that may also be associated with microglial senescence. Microglial specific manipulations of MHC-I in animal models with aging and in AD models are needed to mechanistically understand the role of MHC-I, if any, in the regulation of microglial function in health and disease.

Model		rTg4510 [76]	AppNL-G-F [48]	AppNL-G-F KI [77]	PS2APP [78]	TauPS2APP [78]	APP-SAA (GSE158153)	5X FAD [79]	5X FAD [80]
Method		AutoMACS, RNA-Seq	AutoMACS, RNA-Seq	FACS, scRNA-Seq	FACS, scRNA-Seq	FACS, scRNA-Seq	FACS, RNA-Seq	AutoMACS, RNA-Seq	snRNA-Seq
Age		7 m.o.	8 m.o.	12 m.o.	20-22 m.o.	20-22 m.o.	Not stated	7 m.o.	7 m.o.
Brain Region		Cortex	Cortex	Hippocampus	Hippocampus	Hippocampus	Cortex & Hippocampus	Whole brain	Cortex
Gene	B2m	↑	↑	↑	↑	↑	↑	↑	↑
	H2-D1	↑	↑	↑	↑	↑	↑	↑	↑
	H2-K1	↑	↑	↑	↑	↑	↑	↑	↑
	H2-M3	↑	↑	↑			↑	↑	
	H2-Q6	↑	↑	↑	↑	↑	↑		
	H2-Q7	↑	↑	↑	↑	↑	↑		
	H2-T23	↑	↑	↑	↑	↑	↑		
	Lilrb4	↑	↑		↑	↑	↑	↑	↑
	Pirb	↑					↑		
	Pilra	↑	↑						
	Lilra6	↑							

Table 1: Alterations in MHC-I pathway components and paired immunoglobulin-like receptors in mouse models of AD.

Study		The Mount Sinai Brain Bank (MSBB) study [76]	Cribbs et al., [81]	Rush Alzheimer's Disease Center [80]
Method		RNA-Seq	Microarray	snRNA-Seq
Brain Region		Parahippocampal gyrus	Hippocampus	Prefrontal cortex
Gene	B2m	↑		↑
	HLA-A	↑		↑
	HLA-B	↑	↑	↑
	HLA-C	↑	↑	
	HLA-E	↑	↑	↑
	HLA-F			
	HLA-G		↑	
	Lilrb3/PirB	↑		↑
	Lilrb4	↑		↑
	Pilra	↑		

Table 2: Alterations in MHC-I pathway components and paired immunoglobulin-like receptors in human AD.

Figure 1: MHC-I pathway expression in mouse CNS cell types. Using bulk RNA-Seq data from sorted CNS cell types (~2 m.o.) and from TRAP-Seq data (~3 m.o.) of cell type-specific NuTRAP mice lines, a and b chains of MHC-I and Tap complex components are most highly expressed in microglia with minimal to no expression in astrocytes in astrocytes and neurons.

Figure 2: Microglial MHC-I expression induction with aging but not other cell types. A) Cell type-specific hippocampal RNA from microglial (Cx3cr1^{Litt}-NuTRAP), **B)** astrocytes (Aldh1l1-NuTAP), and **C)** neurons (CamkIIα-NuTAP) was isolated by TRAP. qPCR analysis was performed on Young (3-6M) and Old (18-22M) male and female mice. Increased microglial levels of MHC-I α and β chains and Tap1 were evident in males and females with aging. Minimal or no changes with age were evident in astrocytes and neurons. Two-Way ANOVA (Factors: Age and Sex) with SNK post hoc comparisons (*p<0.05, **p<0.01, ***p<0.001).

Figure 3: Timecourse of microglial MHC-I pathway gene expression with aging. To examine the trajectory of MHC-I gene expression, microglial RNA from female Cx3cr1^{Litt} NuTRAP mice from 12-23 months of age was isolated by TRAP and B2m, H2-D1, H2-K1, H2-M3, and H2-Q6 gene expression examined by qPCR. A steady increase in gene expression was observed for all transcripts (One-Way ANOVA with SNK post hoc comparisons (*p<0.05, **p<0.01).

Figure 4: Cell surface microglial MHC-I protein expression increases with aging. **A)** In young (5-7M) mice (n=6) CD11b^{+}/CD45^{mid} hippocampal singlets were >95% positive for panH2 staining while the negative gate only ~5% of cells were positive One-Way ANOVA with SNK post hoc comparisons (***p<0.001). **B)** In young (5M) and old (24M) males and females panH2 cell surface staining intensity was greater in hippocampal CD11b^{+}/CD45^{mid} singlets as compare to the negative gate and was more intense in old as compared young. T-test,*p<0.05, n=4/age. **C)** This finding was recapitulated with a second panH2 antibody. **D)** Male and female, young (5M) and old (24M) Cx3cr1^{Jung} NuTRAP mouse hippocampal singlets were gated for EGFP and then assessed for panH2 staining intensity. Staining intensity was greater in old as compared to young mice (t-test, *p<0.05).

Figure 5: Microglial B2m induction with aging. In hippocampal sections young, (6 m.o.) and old (21 m.o.) Cx3cr1^{Jung}-NuTRAP mice stained for CD11b and B2m demonstrated qualitative induction of B2m staining in CD11b^{+}/GFP^{+} cells.

Figure 6: MHC-I pathway expression is induced in human microglia with brain aging. A) In re-analysis of whole tissue data from the human GTEx database, induction of alpha chain MHCIs HLA-A, -B, -C, –E, and -F and the invariant beta chain (B2M) is observed in brain, and muscle and lung, but not in circulating blood cells or liver. Pearson's r, ***p<0.001.

B) Examination of human transcriptome patterns by cell nuclei sorting reveals the MHC-I pathway is predominantly expressed by microglia. **C)** In human microglia expression of the MHCI pathway is elevated with aging. n=5 per group, Adult = Ave. 53y.o. Aged = Ave. 93y.o. T-test.

Figure 7: Single cell expression of MHC-I pathway components and receptors. Using public atlas data from the Tabula Muris and Atlas of the Aging Mouse Brain, individual cell co-expression of MHC-I pathway components and potential receptors was examined in **A)** microglia, **B)** astrocytes, and **C)** neurons. In microglia, nearly all cells express MHC-I a and b chains while in astrocytes and neurons only a small portion of cells expressed both components. Additionally potential co-expression of MHC-I receptors Lilra5, Lilrb4, Pilra, and Lilrb3 was examined. A significant portion of microglia demonstrated co-expression of at least one receptor while no receptor expression was observed in astrocytes and neurons. Black circles in the upset plot represent patterns observed in both studies while blue or red circles are patterns only observed in one study.

Figure 8: Cell type specific MHC-I receptor expression. A) Using bulk RNA-Seq data from sorted CNS cell types and from TRAP-Seq data of cell type-specific NuTRAP mice lines MHC-I receptors were nearly solely expressed by microglia. **B-D)** Cell type-specific hippocampal RNA from microglial ($Cx3cr1^{Litt}$), astrocyte (Aldh1l1), and neuronal (CamkIIa) NuTRAP lines was isolated by TRAP. qPCR analysis was performed on Young (3-6M) and Old (18-22M) male and female mice. Increased microglial levels of Lilrb3/PirB, Lilrb4, and Pilra were observed in microglial while no changes or no expression were observed in astrocytes and neurons (Two-Way ANOVA (Factors: Age and Sex) with SNK post hoc comparisons (*p<0.05, **p<0.01, ***p<0.001)). **E)** To examine the trajectory of MHC-I gene expression, microglial RNA from female $Cx3cr1^{Litt}$ NuTRAP mice from 12-23 months of age was isolated by TRAP and Lilrb3/PirB, Lilrb4, and Pilra gene expression examined by qPCR. A steady increase in Lilrb3/PirB and Lilrb4 gene expression was observed for all transcripts (One-Way ANOVA with SNK post hoc comparisons (*p<0.05, **p<0.01)).

Figure 9: MHC-I receptors are induced in human microglia with brain aging. A) In re-analysis of whole tissue data from the human GTEx database, induction of alpha chain MHC-I receptors were increased in the brain with aging and a variety of patterns in other tissues. Pearson's r, ***p<0.001. **B)** Examination of human transcriptome patterns by cell nuclei sorting reveals MHC-I receptors are predominantly expressed by microglia. **C)** In human microglia expression of the MHC-I receptors is elevated with aging. n=5 per group, Adult = Ave. Age 53 Aged = Ave. Age 93. T-test.

Figure 10: APP-PSEN1 hippocampal microglial transcriptome. A) Whole transcriptome pattern of gene expression in CD11b+ hippocampal cells separates between 12 m.o. control and APP-PSEN1 mice. **B)** Clustering of 4,389 differentially expressed genes (t-test, B-H MTC, FC>|1.25|). **C)** Using previously described microglial phenotypic gene expression patterns activation and repression z-scores were generated, indicating expression patterns consistent with increased presence of WAMs, PAMs, MgnDs, IRMs, DAMs, and ARMs. **D)** Gene Set Enrichment Analysis (GSEA) of the non-overlapping phenotypic gene expression sets revealed a similar increased enrichment of ATMs, DAMs, PAMs, and WAMs, while homeostatic patterns were suppressed in APP-PSEN1 as compared to control mice (nominal p-value, *p<0.05, **p<0.01, ***p<0.001) **E)** Examination of specific MHC-I pathway components reveals increased expression of most components in APP-PSEN1 microglia. T-test, *p<0.05, **p<0.01, *** p<0.001.

Figure 11: Aging and Alzheimer's models are associated with increased microglial expression of senescence marker p16. A) Cell type-specific hippocampal RNA from microglial ($Cx3cr1^{Litt}$), astrocyte (Aldh1l1), and neuronal (CamkIIa) NuTRAP lines was isolated by TRAP. qPCR analysis was performed on Young (3-6M) and Old (18-22M) male and female mice for p16. Increased microglial levels of p16 were observed and no detectable p16 transcript was observed in astrocytes and neurons. t-test, ***p<0.001). **B)** Microglial p16 expression as measured by qPCR increased steadily from 12M to 23M of age. One-Way ANOVA with SNK post hoc comparisons (**p<0.01). **C)** MHC-I pathway components, putative receptors, and p16 all correlated across the 12-23M data. **D)** In CD11b+ hippocampal cells from 12 m.o. control and APP-PSEN1 mice also demonstrated increased expression of p16.

Figure 12: MHC-I pathway is enriched for high TREAT-AD target scores. TREAT-AD scores are derived from genetic associations, predicted variant impact, and linkage with dementia-associated phenotypes as well as transcriptomic and proteomic data studies to rank genes for potential investigation in AD studies. MHC-I α and β chain genes and potential non-TCR receptors were compared to all RefSeq genes and found to be over-represented for high scores, which are indicative of higher priority AD targets. By way of comparison well known targets have scores of 6.05 – Trem 2, 5.56 – Apoe, and 5.05 – Tyrobp.

Bibliography

1. Medawar, P.B. Immunity to homologous grafted skin; the fate of skin homografts transplanted to the brain, to subcutaneous tissue, and to the anterior chamber of the eye. *Br J Exp Pathol* **29**, 58-69 (1948).
2. Neuwelt, E.A. & Clark, W.K. Unique aspects of central nervous system immunology. *Neurosurgery* **3**, 419-430 (1978).
3. Galea, I., Bechmann, I. & Perry, V.H. What is immune privilege (not)? *Trends in Immunology* **28**, 12-18 (2007).
4. Ransohoff, R.M. & Cardona, A.E. The myeloid cells of the central nervous system parenchyma. *Nature* **468**, 253-262 (2010).
5. Vincenti, I. & Merkler, D. New advances in immune components mediating viral control in the CNS. *Current Opinion in Virology* **47**, 68-78 (2021).
6. Boulanger, L.M., Huh, G.S. & Shatz, C.J. Neuronal plasticity and cellular immunity: shared molecular mechanisms. *Current Opinion in Neurobiology* **11**, 568-578 (2001).
7. Sheffield, L.G. & Berman, N.E.J. Microglial Expression of MHC Class II Increases in Normal Aging of Nonhuman Primates. *Neurobiology of Aging* **19**, 47-55 (1998).
8. Veerhuis, R., Nielsen, H.M. & Tenner, A.J. Complement in the brain. *Molecular Immunology* **48**, 1592-1603 (2011).
9. Elward, K. & Gasque, P. "Eat me" and "don't eat me" signals govern the innate immune response and tissue repair in the CNS: emphasis on the critical role of the complement system. *Molecular Immunology* **40**, 85-94 (2003).
10. Hanke, Mark L. & Kielian, T. Toll-like receptors in health and disease in the brain: mechanisms and therapeutic potential. *Clinical Science* **121**, 367-387 (2011).
11. Radisky, D.C., Stallings-Mann, M., Hirai, Y. & Bissell, M.J. Single proteins might have dual but related functions in intracellular and extracellular microenvironments. *Nature Reviews Molecular Cell Biology* **10**, 228-234 (2009).
12. Stevens, B.*, et al.* The Classical Complement Cascade Mediates CNS Synapse Elimination. *Cell* **131**, 1164-1178 (2007).
13. Schafer, D.P.*, et al.* Microglia sculpt postnatal neural circuits in an activity and complement-dependent manner. *Neuron* **74**, 691-705 (2012).
14. Glynn, M.W.*, et al.* MHCI negatively regulates synapse density during the establishment of cortical connections. *Nature Neuroscience* **14**, 442-451 (2011).
15. Yoshida, T.M., Wang, A. & Hafler, D.A. Basic principles of neuroimmunology. *Semin Immunopathol* (2022).
16. Croese, T., Castellani, G. & Schwartz, M. Immune cell compartmentalization for brain surveillance and protection. *Nat Immunol* **22**, 1083-1092 (2021).
17. Lampson, L.A. Interpreting MHC class I expression and class I/class II reciprocity in the CNS: reconciling divergent findings. *Microsc Res Tech* **32**, 267-285 (1995).
18. Joly, E., Mucke, L. & Oldstone, M.B. Viral persistence in neurons explained by lack of major histocompatibility class I expression. *Science* **253**, 1283-1285 (1991).
19. Wong, G.H., Bartlett, P.F., Clark-Lewis, I., Battye, F. & Schrader, J.W. Inducible expression of H-2 and Ia antigens on brain cells. *Nature* **310**, 688-691 (1984).
20. Shatz, C.J. MHC class I: an unexpected role in neuronal plasticity. *Neuron* **64**, 40-45 (2009).
21. Rodgers, J.R. & Cook, R.G. MHC class Ib molecules bridge innate and acquired immunity. *Nature Reviews Immunology* **5**, 459-471 (2005).
22. Shiina, T., Blancher, A., Inoko, H. & Kulski, J.K. Comparative genomics of the human, macaque and mouse major histocompatibility complex. *Immunology* **150**, 127-138 (2017).
23. Ioannidu, S., Walter, L., Dressel, R. & Gunther, E. Physical map and expression profile of genes of the telomeric class I gene region of the rat MHC. *J Immunol* **166**, 3957-3965 (2001).
24. Shastri, N., Schwab, S. & Serwold, T. Producing nature's gene-chips: the generation of peptides for display by MHC class I molecules. *Annu Rev Immunol* **20**, 463-493 (2002).
25. Cruz, F.M., Colbert, J.D., Merino, E., Kriegsman, B.A. & Rock, K.L. The Biology and Underlying Mechanisms of Cross-Presentation of Exogenous Antigens on MHC-I Molecules. *Annu Rev Immunol* **35**, 149-176 (2017).
26. York, I.A.R., K.L. ANTIGEN PROCESSING AND PRESENTATION BY THE CLASS I MAJOR HISTOCOMPATIBILITY COMPLEX. *Annual Review of Immunology* **14**, 369-396 (1996).
27. Rossjohn, J.*, et al.* T cell antigen receptor recognition of antigen-presenting molecules. *Annu Rev Immunol* **33**, 169-200 (2015).

28. Barrow, A.D. & Trowsdale, J. The extended human leukocyte receptor complex: diverse ways of modulating immune responses. *Immunol Rev* **224**, 98-123 (2008).
29. Burshtyn, D.N. & Morcos, C. The Expanding Spectrum of Ligands for Leukocyte Ig-like Receptors. *J Immunol* **196**, 947-955 (2016).
30. Borges, L., Hsu, M.L., Fanger, N., Kubin, M. & Cosman, D. A family of human lymphoid and myeloid Ig-like receptors, some of which bind to MHC class I molecules. *J Immunol* **159**, 5192-5196 (1997).
31. Marffy, A.L. & McCarthy, A.J. Leukocyte Immunoglobulin-Like Receptors (LILRs) on Human Neutrophils: Modulators of Infection and Immunity. *Front Immunol* **11**, 857 (2020).
32. Hudson, L.E. & Allen, R.L. Leukocyte Ig-Like Receptors - A Model for MHC Class I Disease Associations. *Front Immunol* **7**, 281 (2016).
33. Takai, T. Paired immunoglobulin-like receptors and their MHC class I recognition. *Immunology* **115**, 433-440 (2005).
34. Foster, A.J., Bird, J.H., Timmer, M.S.M. & Stocker, B.L. The Ligands of C-Type Lectins. in *C-Type Lectin Receptors in Immunity* (ed. Yamasaki, S.) 191-215 (Springer Japan, Tokyo, 2016).
35. Getahun, A. & Cambier, J.C. Of ITIMs, ITAMs, and ITAMis: revisiting immunoglobulin Fc receptor signaling. *Immunol Rev* **268**, 66-73 (2015).
36. Neumann, H., Schmidt, H., Cavalie, A., Jenne, D. & Wekerle, H. Major histocompatibility complex (MHC) class I gene expression in single neurons of the central nervous system: differential regulation by interferon (IFN)-gamma and tumor necrosis factor (TNF)-alpha. *J Exp Med* **185**, 305-316 (1997).
37. Adelson, J.D.*, et al.* Neuroprotection from stroke in the absence of MHCI or PirB. *Neuron* **73**, 1100-1107 (2012).
38. Yong, V.W. & Antel, J.P. Major histocompatibility complex molecules on glial cells. *Seminars in Neuroscience* **4**, 231-240 (1992).
39. Needleman, L.A., Liu, X.B., El-Sabeawy, F., Jones, E.G. & McAllister, A.K. MHC class I molecules are present both pre- and postsynaptically in the visual cortex during postnatal development and in adulthood. *Proc Natl Acad Sci U S A* **107**, 16999-17004 (2010).
40. Huh, G.S.*, et al.* Functional requirement for class I MHC in CNS development and plasticity. *Science* **290**, 2155-2159 (2000).
41. Corriveau, R.A., Huh, G.S. & Shatz, C.J. Regulation of class I MHC gene expression in the developing and mature CNS by neural activity. *Neuron* **21**, 505-520 (1998).
42. Syken, J., Grandpre, T., Kanold, P.O. & Shatz, C.J. PirB restricts ocular-dominance plasticity in visual cortex. *Science* **313**, 1795-1800 (2006).
43. Zalocusky, K.A.*, et al.* Neuronal ApoE upregulates MHC-I expression to drive selective neurodegeneration in Alzheimer's disease. *Nature Neuroscience* **24**, 786-798 (2021).
44. Rostami, J.*, et al.* Astrocytes have the capacity to act as antigen-presenting cells in the Parkinson's disease brain. *Journal of Neuroinflammation* **17**, 119 (2020).
45. Goddery, E.N.*, et al.* Microglia and Perivascular Macrophages Act as Antigen Presenting Cells to Promote CD8 T Cell Infiltration of the Brain. *Front Immunol* **12**, 726421 (2021).
46. Truong, P., Heydari, S., Garidou, L. & McGavern, D.B. Persistent viral infection elevates central nervous system MHC class I through chronic production of interferons. *J Immunol* **183**, 3895-3905 (2009).
47. Holtman, I.R.*, et al.* Induction of a common microglia gene expression signature by aging and neurodegenerative conditions: a co-expression meta-analysis. *Acta Neuropathologica Communications* **3**, 31 (2015).
48. Sobue, A.*, et al.* Microglial gene signature reveals loss of homeostatic microglia associated with neurodegeneration of Alzheimer's disease. *Acta Neuropathologica Communications* **9**, 1 (2021).
49. Krasemann, S.*, et al.* The TREM2-APOE Pathway Drives the Transcriptional Phenotype of Dysfunctional Microglia in Neurodegenerative Diseases. *Immunity* **47**, 566-581 e569 (2017).
50. Paolicelli, R.C.*, et al.* Microglia states and nomenclature: A field at its crossroads. *Neuron* **110**, 3458-3483 (2022).
51. Mangold, C.A.*, et al.* CNS-wide Sexually Dimorphic Induction of the Major Histocompatibility Complex 1 Pathway With Aging. *J Gerontol A Biol Sci Med Sci* **72**, 16-29 (2017).
52. VanGuilder Starkey, H.D.*, et al.* Neuroglial expression of the MHCI pathway and PirB receptor is upregulated in the hippocampus with advanced aging. *J Mol Neurosci* **48**, 111-126 (2012).
53. Chucair-Elliott, A.J.*, et al.* Inducible cell-specific mouse models for paired epigenetic and transcriptomic studies of microglia and astroglia. *Commun Biol* **3**, 693 (2020).

54. Srinivasan, R., *et al.* New Transgenic Mouse Lines for Selectively Targeting Astrocytes and Studying Calcium Signals in Astrocyte Processes In Situ and In Vivo. *Neuron* **92**, 1181-1195 (2016).
55. Yona, S., *et al.* Fate mapping reveals origins and dynamics of monocytes and tissue macrophages under homeostasis. *Immunity* **38**, 79-91 (2013).
56. Parkhurst, C.N., *et al.* Microglia promote learning-dependent synapse formation through brain-derived neurotrophic factor. *Cell* **155**, 1596-1609 (2013).
57. Madisen, L., *et al.* A robust and high-throughput Cre reporting and characterization system for the whole mouse brain. *Nat Neurosci* **13**, 133-140 (2010).
58. Roh, H.C., *et al.* Simultaneous Transcriptional and Epigenomic Profiling from Specific Cell Types within Heterogeneous Tissues In Vivo. *Cell Rep* **18**, 1048-1061 (2017).
59. Jankowsky, J.L., *et al.* Mutant presenilins specifically elevate the levels of the 42 residue beta-amyloid peptide in vivo: evidence for augmentation of a 42-specific gamma secretase. *Hum Mol Genet* **13**, 159-170 (2004).
60. Vartak, R.S., Rodin, A. & Oddo, S. Differential activation of the mTOR/autophagy pathway predicts cognitive performance in APP/PS1 mice. *Neurobiol Aging* **83**, 105-113 (2019).
61. Chucair-Elliott, A.J., *et al.* Tamoxifen induction of Cre recombinase does not cause long-lasting or sexually divergent responses in the CNS epigenome or transcriptome: implications for the design of aging studies. *Geroscience* **41**, 691-708 (2019).
62. Sahasrabuddhe, V. & Ghosh, H.S. Cx3Cr1-Cre induction leads to microglial activation and IFN-1 signaling caused by DNA damage in early postnatal brain. *Cell Rep* **38**, 110252 (2022).
63. Ocañas, S.R., *et al.* Differential Regulation of Mouse Hippocampal Gene Expression Sex Differences by Chromosomal Content and Gonadal Sex. *Molecular Neurobiology* **59**, 4669-4702 (2022).
64. Masser, D.R., *et al.* Hippocampal subregions exhibit both distinct and shared transcriptomic responses to aging and nonneurodegenerative cognitive decline. *J Gerontol A Biol Sci Med Sci* **69**, 1311-1324 (2014).
65. Ocanas, S.R., *et al.* Minimizing the Ex Vivo Confounds of Cell-Isolation Techniques on Transcriptomic and Translatomic Profiles of Purified Microglia. *eNeuro* **9**(2022).
66. Almanzar, N., *et al.* A single-cell transcriptomic atlas characterizes ageing tissues in the mouse. *Nature* **583**, 590-595 (2020).
67. Ximerakis, M., *et al.* Single-cell transcriptomic profiling of the aging mouse brain. *Nature Neuroscience* **22**, 1696-1708 (2019).
68. Virtanen, P., *et al.* SciPy 1.0: fundamental algorithms for scientific computing in Python. *Nature Methods* **17**, 261-272 (2020).
69. Zhang, Y., *et al.* An RNA-sequencing transcriptome and splicing database of glia, neurons, and vascular cells of the cerebral cortex. *J Neurosci* **34**, 11929-11947 (2014).
70. Heiman, M., Kulicke, R., Fenster, R.J., Greengard, P. & Heintz, N. Cell type–specific mRNA purification by translating ribosome affinity purification (TRAP). *Nature Protocols* **9**, 1282-1291 (2014).
71. Vasek, M.J., *et al.* Microglia perform local protein synthesis at perisynaptic and phagocytic structures. *bioRxiv*, 2021.2001.2013.426577 (2021).
72. Stallcup, K.C., Springer, T.A. & Mescher, M.F. Characterization of an anti-H-2 monoclonal antibody and its use in large-scale antigen purification. *J Immunol* **127**, 923-930 (1981).
73. GTEx-Consortium. The Genotype-Tissue Expression (GTEx) project. *Nat Genet* **45**, 580-585 (2013).
74. Zhang, Y., *et al.* Purification and Characterization of Progenitor and Mature Human Astrocytes Reveals Transcriptional and Functional Differences with Mouse. *Neuron* **89**, 37-53 (2016).
75. Olah, M., *et al.* A transcriptomic atlas of aged human microglia. *Nature Communications* **9**, 539 (2018).
76. Wang, M., *et al.* The Mount Sinai cohort of large-scale genomic, transcriptomic and proteomic data in Alzheimer's disease. *Sci Data* **5**, 180185 (2018).
77. Sala Frigerio, C., *et al.* The Major Risk Factors for Alzheimer's Disease: Age, Sex, and Genes Modulate the Microglia Response to Abeta Plaques. *Cell Rep* **27**, 1293-1306 e1296 (2019).
78. Lee, S.H., *et al.* TREM2-independent oligodendrocyte, astrocyte, and T cell responses to tau and amyloid pathology in mouse models of Alzheimer disease. *Cell Rep* **37**, 110158 (2021).
79. Baik, S.H., *et al.* A Breakdown in Metabolic Reprogramming Causes Microglia Dysfunction in Alzheimer's Disease. *Cell Metab* **30**, 493-507 e496 (2019).
80. Zhou, Y., *et al.* Human and mouse single-nucleus transcriptomics reveal TREM2-dependent and TREM2-independent cellular responses in Alzheimer's disease. *Nat Med* **26**, 131-142 (2020).

81. Cribbs, D.H., *et al.* Extensive innate immune gene activation accompanies brain aging, increasing vulnerability to cognitive decline and neurodegeneration: a microarray study. *J Neuroinflammation* **9**, 179 (2012).
82. Cary, G., *et al.* Genetic and Multi-omic Risk Assessment of Alzheimer's Disease Implicates Core Associated Biological Domains. *medRxiv*, 2022.2012.2015.22283478 (2022).
83. Town, T., Tan, J., Flavell, R.A. & Mullan, M. T-cells in Alzheimer's disease. *Neuromolecular Med* **7**, 255-264 (2005).
84. Gemechu, J.M. & Bentivoglio, M. T Cell Recruitment in the Brain during Normal Aging. *Front Cell Neurosci* **6**, 38 (2012).
85. Unger, M.S., *et al.* CD8(+) T-cells infiltrate Alzheimer's disease brains and regulate neuronal- and synapse-related gene expression in APP-PS1 transgenic mice. *Brain Behav Immun* **89**, 67-86 (2020).
86. Jorfi, M., Maaser-Hecker, A. & Tanzi, R.E. The neuroimmune axis of Alzheimer's disease. *Genome Med* **15**, 6 (2023).
87. Navarro Negredo, P. & Brunet, A. Unwanted help from T cells in the aging central nervous system. *Nature Aging* **1**, 330-331 (2021).
88. Proescholdt, M.G., *et al.* Intracerebroventricular but not intravenous interleukin-1beta induces widespread vascular-mediated leukocyte infiltration and immune signal mRNA expression followed by brain-wide glial activation. *Neuroscience* **112**, 731-749 (2002).
89. Batterman, K.V., Cabrera, P.E., Moore, T.L. & Rosene, D.L. T Cells Actively Infiltrate the White Matter of the Aging Monkey Brain in Relation to Increased Microglial Reactivity and Cognitive Decline. *Front Immunol* **12**, 607691 (2021).
90. Groh, J., *et al.* Accumulation of cytotoxic T cells in the aged CNS leads to axon degeneration and contributes to cognitive and motor decline. *Nature Aging* **1**, 357-367 (2021).
91. Berry, K., *et al.* B and T Lymphocyte Densities Remain Stable With Age in Human Cortex. *ASN Neuro* **13**, 17590914211018117 (2021).
92. Zhang, X., *et al.* Aged microglia promote peripheral T cell infiltration by reprogramming the microenvironment of neurogenic niches. *Immunity & Ageing* **19**, 34 (2022).
93. Allen, W.E., Blosser, T.R., Sullivan, Z.A., Dulac, C. & Zhuang, X. Molecular and spatial signatures of mouse brain aging at single-cell resolution. *Cell* **186**, 194-208 e118 (2023).
94. Benakis, C., *et al.* T cells modulate the microglial response to brain ischemia. *Elife* **11**(2022).
95. Altendorfer, B., *et al.* Transcriptomic Profiling Identifies CD8(+) T Cells in the Brain of Aged and Alzheimer's Disease Transgenic Mice as Tissue-Resident Memory T Cells. *J Immunol* **209**, 1272-1285 (2022).
96. Rustenhoven, J., *et al.* Functional characterization of the dural sinuses as a neuroimmune interface. *Cell* **184**, 1000-1016 e1027 (2021).
97. Dulken, B.W., *et al.* Single-cell analysis reveals T cell infiltration in old neurogenic niches. *Nature* **571**, 205-210 (2019).
98. Haure-Mirande, J.-V., Audrain, M., Ehrlich, M.E. & Gandy, S. Microglial TYROBP/DAP12 in Alzheimer's disease: Transduction of physiological and pathological signals across TREM2. *Molecular Neurodegeneration* **17**, 55 (2022).
99. Ennerfelt, H., *et al.* SYK coordinates neuroprotective microglial responses in neurodegenerative disease. *Cell* **185**, 4135-4152 e4122 (2022).
100. Schafer, D.P. & Stillman, J.M. Microglia are SYK of Abeta and cell debris. *Cell* **185**, 4043-4045 (2022).
101. Wang, S., *et al.* TREM2 drives microglia response to amyloid-beta via SYK-dependent and -independent pathways. *Cell* **185**, 4153-4169 e4119 (2022).
102. Shiroishi, M., *et al.* Structural basis for recognition of the nonclassical MHC molecule HLA-G by the leukocyte Ig-like receptor B2 (LILRB2/LIR2/ILT4/CD85d). *Proc Natl Acad Sci U S A* **103**, 16412-16417 (2006).
103. Pluvinage, J.V., *et al.* CD22 blockade restores homeostatic microglial phagocytosis in ageing brains. *Nature* **568**, 187-192 (2019).
104. Pereira, B.I., *et al.* Senescent cells evade immune clearance via HLA-E-mediated NK and CD8+ T cell inhibition. *Nature Communications* **10**, 2387 (2019).
105. Stojiljkovic, M.R., *et al.* Phenotypic and functional differences between senescent and aged murine microglia. *Neurobiol Aging* **74**, 56-69 (2019).
106. Streit, W.J. Microglial senescence: does the brain's immune system have an expiration date? *Trends Neurosci* **29**, 506-510 (2006).

107. Gems, D. & Kern, C.C. Is "cellular senescence" a misnomer? *Geroscience* **44**, 2461-2469 (2022).

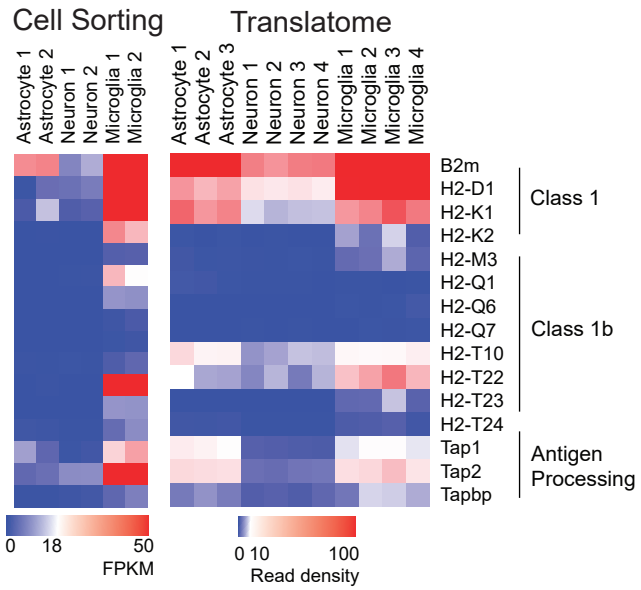

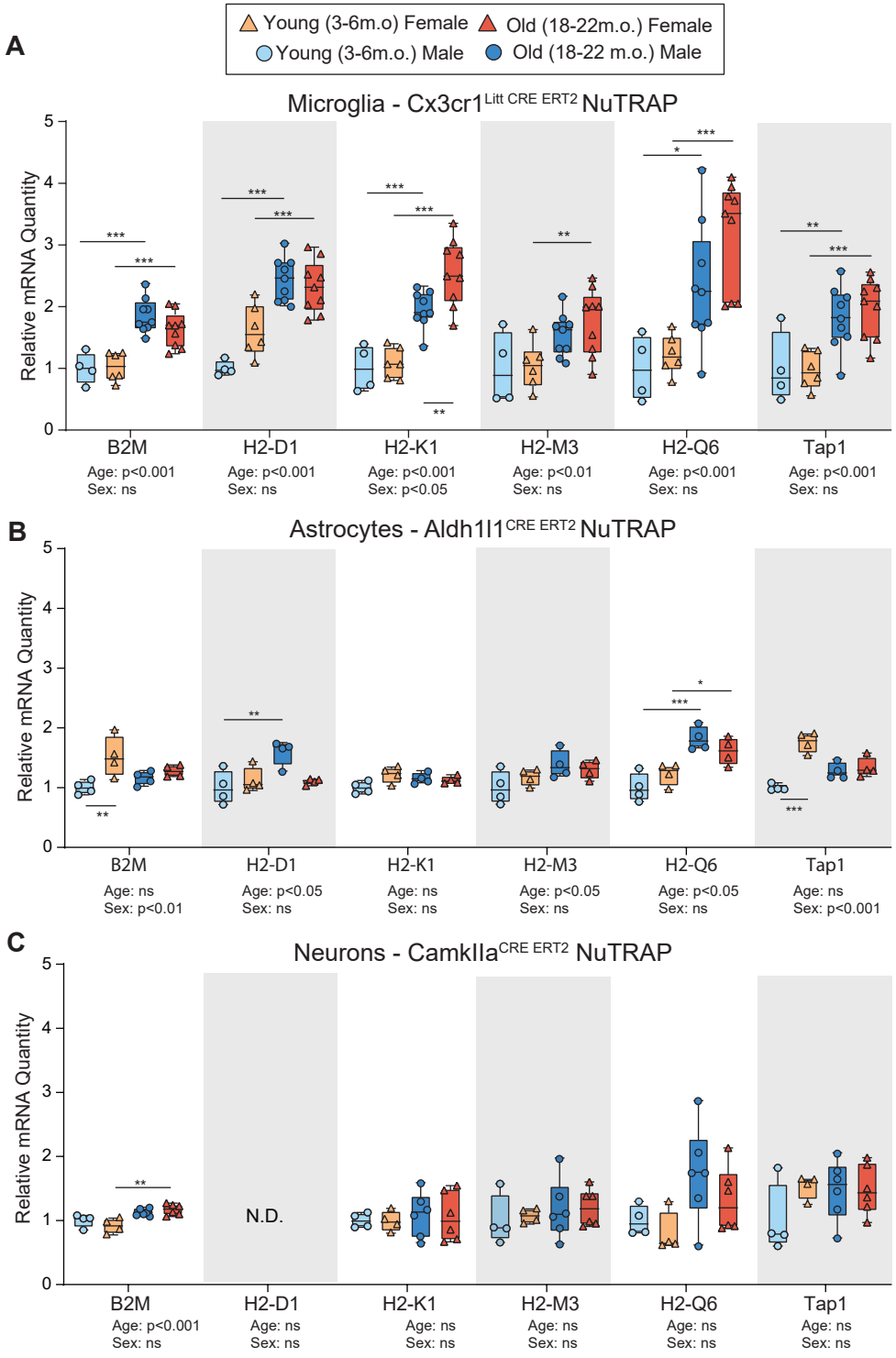

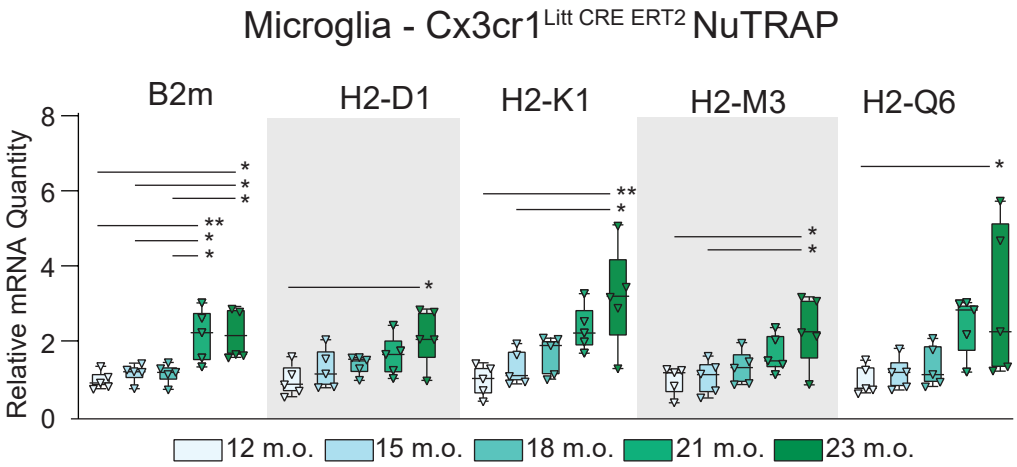

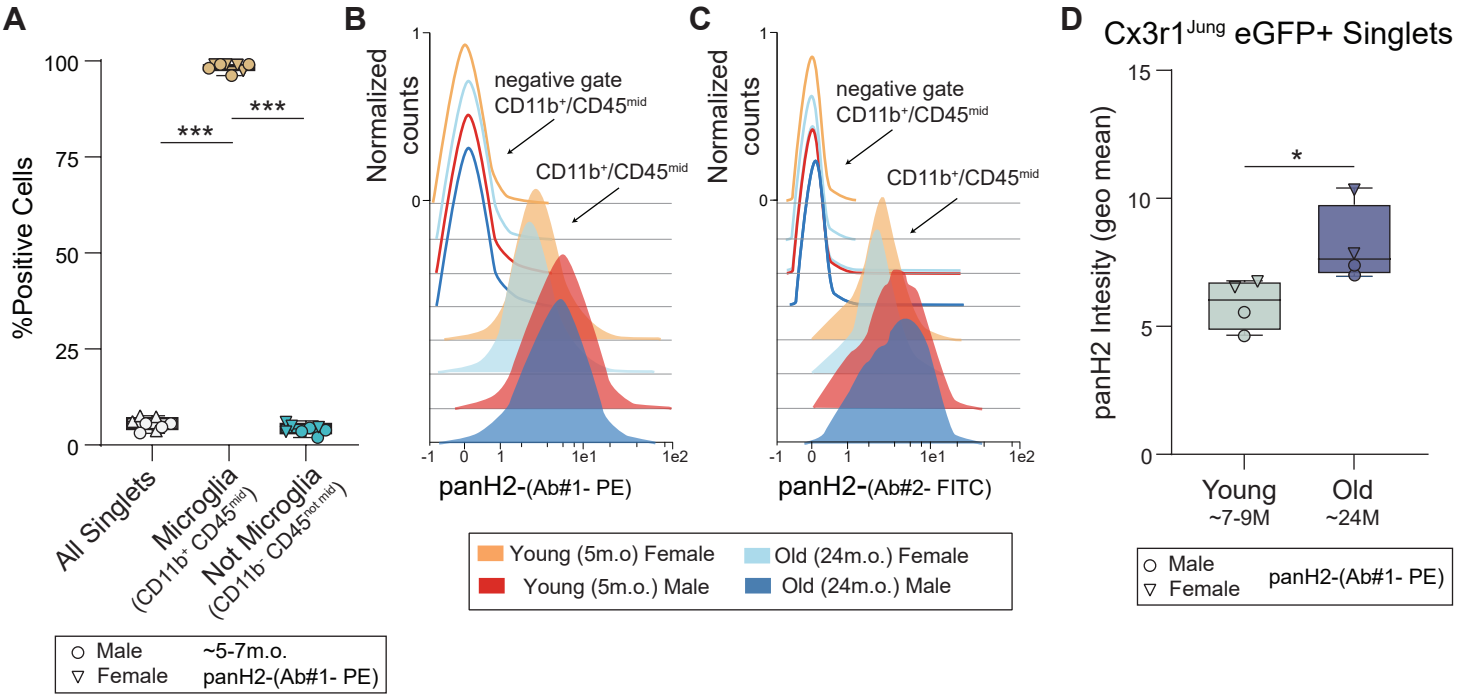

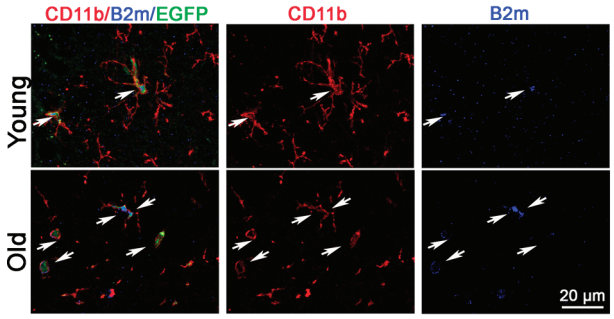

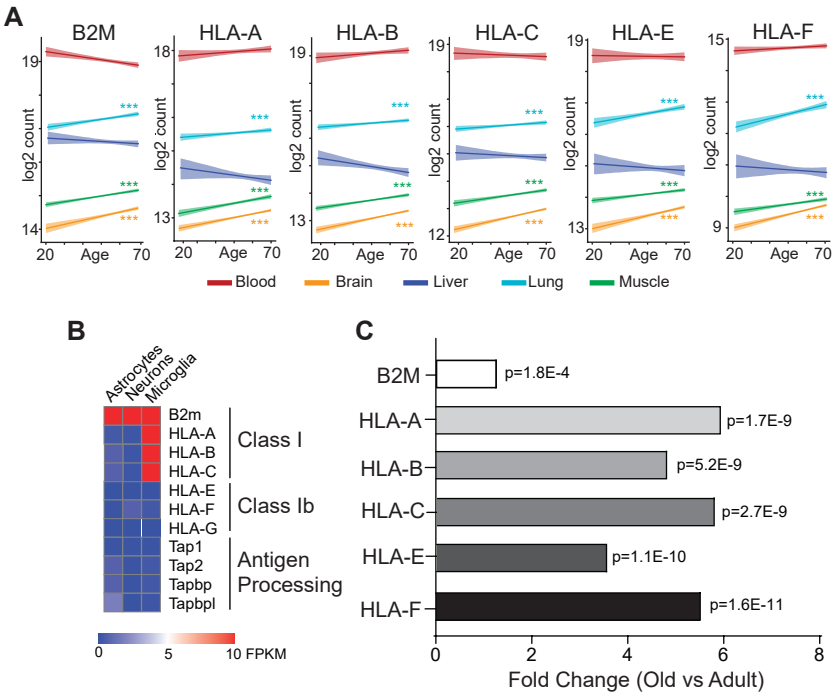

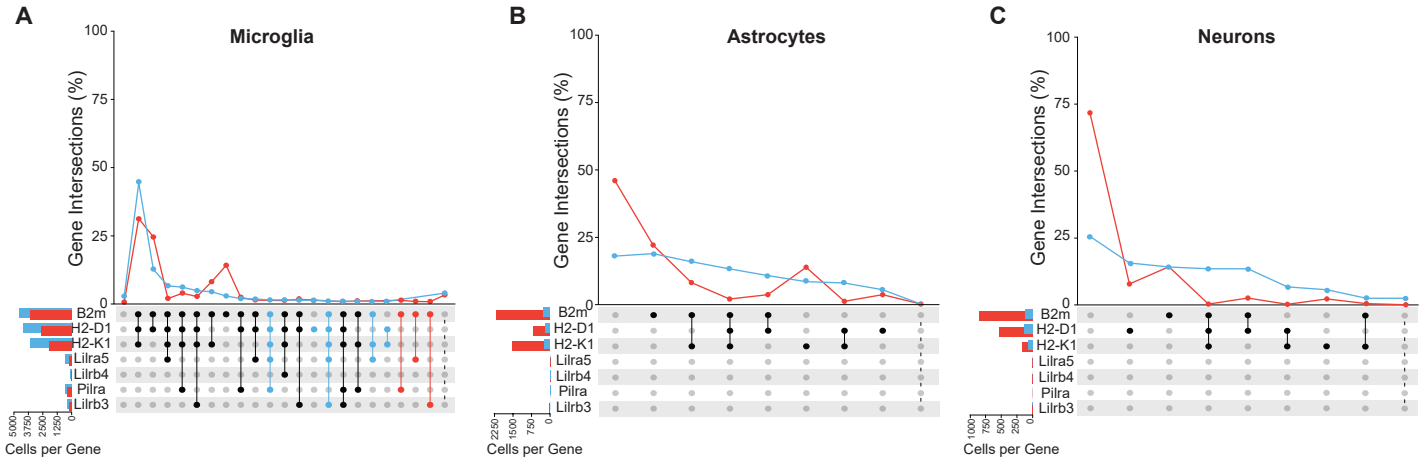

Tabula Muris Consortium Atlas of the Aging Mouse Brain